electronics

Article

Mixed Near-Field and Far-Field Sources Localization via Oblique Projection

Heping Shi *, Yanjie Yang, Guanghui Yan and Shaohua Wang

School of Automobile and Transportation, Tianjin University of Technology and Education, Tianjin 300222, China; yanjie_yang@tute.edu.cn (Y.Y.); yanguanghui@tute.edu.cn (G.Y.); shaohuawang@tute.edu.cn (S.W.)
* Correspondence: shiheping@tju.edu.cn

Abstract: This paper presents a novel mixed source localization algorithm based on high-order cumulant (HOC) and oblique projection techniques. To address the issue of lower accuracy in near-field source (NFS) localization compared to the far-field source (FFS) localization, the presented algorithm further enhances the accuracy of NFS localization. First, the FFS's direction-of-arrival (DOA) estimate is acquired utilizing a multiple signal classification (MUSIC) spectral peak search. To classify mixed sources more effectively, we utilize the oblique projection technique, which can successfully prevent FFS information from influencing the estimation of NFS parameters. A HOC matrix with solely NFS DOA information is built by choosing array elements in a specific sequence. The estimation of the NFS DOA is then derived using the estimation of signal parameters via a rotational invariance technique (ESPRIT)-like algorithm. Finally, the NFS range is acquired by a MUSIC search. The performance of the presented algorithm is discussed in several aspects. Compared to existing matrix difference methods, the presented algorithm, which adopts the oblique projection method, achieves superior results in the separation of mixed sources. Without excessively increasing the computational complexity, it not only ensures the performance of localization parameter estimation for FFS but also estimates the NFS with higher precision. The numerical simulations attest to the superior performance of the presented algorithm.

Keywords: mixed sources localization; symmetric uniform array; oblique projection; high-order cumulant

Citation: Shi, H.; Yang, Y.; Yan, G.; Wang, S. Mixed Near-Field and Far-Field Sources Localization via Oblique Projection. *Electronics* **2023**, *12*, 2340. https://doi.org/10.3390/electronics12102340

Academic Editors: Costas Psychalinos and Jianfeng Li

Received: 17 April 2023
Revised: 13 May 2023
Accepted: 19 May 2023
Published: 22 May 2023

1. Introduction

Source localization [1,2], which has garnered significant research attention in the field of array signal processing, plays a crucial role in various military and civil domains. These domains include radar, wireless communication, sonar, and seismic exploration, among many others [3]. Pure FFS algorithms were the primary focus of early source localization studies. The MUSIC [4] and ESPRIT [5] algorithms are the two most often used FFS localization methods. As the range between the FFS and the array can be thought to be limitless, the wavefront of the FFS is considered to be roughly planar. However, given that the NFS is positioned in the Fresnel area [6], where the incident wavefront curvature cannot be disregarded, its wavefront is a spherical wavefront. Pure FFS methods are not applicable to NFS scenarios because the models established by the two types of sources are different. In addition to the DOA, NFS methods also need to obtain the range parameter. As a consequence, many academics have conducted extensive studies on pure NFS algorithms [7,8]. However, sensor arrays can receive more than just a single type of signal. With the development of practical application scenarios such as radar and microphones, academics have found that the signals could come from a combination of FFS and NFS. The NFS localization parameters might not be accurately determined if pure FFS algorithms are applied to the mixed sources. When a pure NFS algorithm is applied to mixed sources, it will produce issues including excessive algorithm computation and the inability to separate the mixed sources. Therefore, there is a need to research an algorithm that can accurately estimate the FFS DOA, NFS DOA, and NFS range simultaneously. It is of important practical significance to develop mixed NFS and FFS localization algorithms.

In order to tackle the localization problem for mixed sources, numerous methods have been presented. Based on the HOC technique, a two-stage MUSIC (TSMUSIC) algorithm was presented in [9]. In this algorithm, two special HOC matrices are constructed, and it performs MUSIC spectral peak searches twice. Consequently, there is a heavy burden in terms of computation. A MUSIC-based one-dimensional search (MBODS) method based on the oblique projection technique was proposed in [10]. It uses only second-order statistical properties to obtain an estimate of FFS DOA using the MUSIC spectral peak search. Consequently, it suppresses the FFS component by oblique projection. The algorithm has less computational complexity but only utilizes the inverse diagonal information of the covariance matrix, and there is an array aperture loss. A subspace difference-based localization algorithm was presented in [11]. By conducting covariance matrix reconstruction after separating the NFS component from the signal subspace on the basis of obtaining the FFS localization parameter, the algorithm is more effective in classifying mixed sources. A mixed source localization method based on HOC was proposed in [12]. It divides the symmetric uniform linear array into two subarrays and obtains the mixed source localization parameters by the HOC technique and polynomial decomposition method without spectral peak searching. A mixed-order statistics-based (MOS) localization algorithm was proposed by Zheng et al. in [13]. After acquiring the DOA of the FFS through MUSIC spectral peak search, it utilizes the matrix difference approach to obtain the NFS component of the HOC matrix. Finally, the DOA of NFS is acquired through high-order MUSIC spectral peak searches. Due to its use of HOC matrices and several MUSIC spectral peak searches, it has excessively high computational complexity.

A localization method based on cumulant matrix reconstruction (CMR) was proposed in [14]. Based on the HOC kurtosis of the FFS, the algorithm applies the difference method to gain the NFS components. The DOA of the NFS is obtained utilizing the ESPRIT-like algorithm [15], which reduces the spectral peak search compared to the MOS algorithm. The high-order difference localization algorithm (HODA) [16] was presented by Molaei. The electrical angles of the NFS are calculated by the difference method with several HOC matrices and compared to the initial DOA set obtained by the ESPRIT-like algorithm. Next, a kurtosis test is used to obtain the FFS DOA, and it can correctly distinguish the mixed sources with the same DOA. A cross-array-based mixed source localization algorithm [17] extends the one-dimension DOA estimation to two dimensions. The Vandermonde decomposition is implemented to estimate the DOA, and range information is gained by the l_1-norm minimization problem. This method can effectively avoid array aperture loss. Yin proposed a mixed sources localization method based on a concentric orthogonal loop and dipole array [18]. A noise-free covariance matrix is constructed. Additionally, a rough estimation of the localization parameters is obtained using the subarray partitioning method in the spatially accurate model. Then, MUSIC spectral peak search is performed near the rough values of the parameter estimates to obtain the exact values.

To estimate the mixed source localization parameters, most of the aforementioned algorithms use the properties of the eigen subspace with a uniform linear array model. Wang et al. first applied sparse theory to the mixed source localization algorithm [19] in order to increase the estimation accuracy. The DOA is estimated using the weighted l_1-norm method by building a HOC matrix just about the angular factor. Next, sparse reconstruction is applied to acquire the range information of the NFS. Based on the nested array and compressive sensing methods, Tian proposed a mixed sources parameter estimation method [20]. It showed some improvement in estimation accuracy, but the use of HOC leads to the higher computational complexity of the algorithm. Zheng presented a mixed source localization method using a symmetric nested array as the foundation [21]. In the algorithm, the NFS components are separated by the oblique projection method, and the DOA estimation of the NFS is acquired by the spatial smoothing MUSIC method.

Although the estimation performance of the sparse reconstruction class of algorithms is superior, there is the inevitable problem of large computational complexity.

The majority of these methods also perform well in terms of estimating FFS DOA, but the precision of NFS localization parameters is slightly poorer in comparison. Thus, a mixed source localization method is provided in this paper that combines the oblique projection technique and HOC theory. This method improves the performance of NFS estimation while essentially maintaining the performance of FFS localization. The main contributions of this paper are as follows:

(1) We combine oblique projection, HOC, and ESPRIT-like methods to effectively separate mixed sources. This also leads to improved accuracy of the NFS localization parameters. (2) We perform a detailed analysis of the proposed algorithm's maximum estimated number of sources, estimation accuracy, and computational complexity. The structure of the paper is as follows: The mixed-source reception model is described in Section 2. Section 3 gives a detailed explanation of the derivation and procedures of the presented algorithm and a discussion of its performance. Simulations are described in Section 4. The conclusion is put forward in Section 5.

Notation: Vectors are denoted by bold lowercase letters, while bold capital letters are used to indicate matrices. The matrix's complex conjugate, transposition, conjugate transpose, inverse, and pseudo-inverse are indicated by superscript *, T, H, -1, and †, respectively. The expectation operation is denoted by $\mathrm{E}\{\cdot\}$. The $m \times n$-dimensional complex matrix space is represented by $\mathbb{C}^{m \times n}$. $\mathbf{I}_m$ denotes the $m \times m$-dimensional identity matrix. The operation $\mathrm{diag}\{\cdot\}$ represents the diagonal matrix.

2. Mathematical Data Model

It is assumed that there are $L = 2M + 1$ omnidirectional array elements to form a uniform linear array. The central array element is selected as the phase reference point. And the uniform linear array is incident by K mixed NFSs and FFSs, of which the first K_1 signals are the FFSs and $(K - K_1)$ signals are the NFSs. The array element spacing is indicated by d, and the spacing satisfies $d = \lambda/4$, where λ represents the signal wavelength. The angle of the kth incident source is denoted by θ_k and satisfies $-90^\circ \leq \theta_k \leq 90^\circ$. Then, the expression of the source data received from the mth array element is:

$$x_m(t) = \sum_{k=1}^{K} s_k(t) e^{j\tau_{mk}} + n_m(t) \tag{1}$$

where $-M \leq m \leq M$, and s_k denotes the complex envelope of the mixed source; τ_{mk} denotes the propagation delay between the kth signal incident and the reference array and mth array elements; and $n_m(t)$ represents the additive Gaussian white noise of the mth array element. The propagation delay of NFS can be approximated by Fresnel as:

$$\tau_{mk} \approx m\gamma_k + m^2\phi_k \tag{2}$$

where

$$\gamma_k = -2\pi \frac{d}{\lambda} \sin\theta_k \tag{3}$$

$$\phi_k = \pi \frac{d^2}{\lambda r_k} \cos^2\theta_k \tag{4}$$

where r_k is the range between the kth signal and the central array element. r_k must satisfy the condition $0.62(D^3/\lambda)^{1/2} \leq r_k \leq 2D^2/\lambda$, where D indicates the array aperture, and the array aperture of the signal reception model in this paper is $D = 2Md$.

In addition, when the incident signal is FFS, which means that the signal position is outside the Fresnel region, its range can be considered infinite at this time. According to Equation (4), we can obviously obtain $\phi_k = 0$. The expression of FFS propagation delay τ_{mk} is:

$$\tau_{mk} \approx m\gamma_k \tag{5}$$

The snapshot data with 2M + 1 array elements is expressed as:

$$\begin{aligned}\mathbf{x}(t) &= \mathbf{A}\mathbf{s}(t) + \mathbf{n}(t) \\ &= \mathbf{A}_F\mathbf{s}_F(t) + \mathbf{A}_N\mathbf{s}_N(t) + \mathbf{n}(t)\end{aligned} \tag{6}$$

where

$$\mathbf{x}(t) = [x_{-M}(t), \ldots, x_0(t), \ldots, x_M(t)]^T \in \mathbb{C}^{(2M+1)\times 1} \tag{7}$$

$$\mathbf{A}_F = \left[\mathbf{a}_F(\theta_1), \ldots, \mathbf{a}_F(\theta_{K_1})\right] \in \mathbb{C}^{(2M+1)\times K_1} \tag{8}$$

$$\mathbf{A}_N = \left[\mathbf{a}_N(\theta_{K_1+1}, r_{K_1+1}), \ldots, \mathbf{a}_N(\theta_K, r_K)\right] \in \mathbb{C}^{(2M+1)\times(K-K_1)} \tag{9}$$

$$\mathbf{s}_F(t) = \left[s_1(t), \ldots, s_{K_1}(t)\right]^T \in \mathbb{C}^{K_1\times 1} \tag{10}$$

$$\mathbf{s}_N(t) = \left[s_{K_1+1}(t), \ldots, s_K(t)\right]^T \in \mathbb{C}^{(K-K_1)\times 1} \tag{11}$$

$$\mathbf{n}(t) = [n_{-M}(t), \ldots, n_0(t), \ldots, n_M(t)]^T \in \mathbb{C}^{(2M+1)\times 1} \tag{12}$$

where $\mathbf{A}_F$ and $\mathbf{A}_N$ are the manifold matrices; $\mathbf{s}_F(t)$ and $\mathbf{s}_N(t)$ are the signal vectors of the FFS and NFS, respectively, and $\mathbf{n}(t)$ represents the noise vector; and

$$\mathbf{a}_F(\theta_k) = \left[e^{j(-M\gamma_k)}, e^{j[(-M+1)\gamma_k]}, \ldots, 1, \ldots, e^{j(M\gamma_k)}\right]^T, \tag{13}$$

$$\mathbf{a}_N(\theta_k, r_k) = \left[e^{j(-M\gamma_k+M^2\phi_k)}, e^{j[(-M+1)\gamma_k+(-M+1)^2\phi_k]}, \ldots, 1, \ldots, e^{j(M\gamma_k+M^2\phi_k)}\right]^T, \tag{14}$$

are the (2M + 1) × 1 dimensional steering vectors of the FFS and NFS, respectively.

Additionally, the following assumptions are made about the model in this paper.

(1) The sources are non-Gaussian narrowband stationary processes with non-zero kurtosis and a zero mean. Each source needs to be independent of the others.
(2) The noise is additive zero-mean Gaussian white noise that is statistically independent of the source.
(3) The number of incident signals must be smaller than the number of array elements. Moreover, the number of signals is known and can be determined utilizing the MDL or AIC criterion, among other techniques.

3. The Proposed Procedure

3.1. DOA Estimation for FFS

The covariance matrix $\mathbf{R}$ of the received data from the uniform linear array is eigendecomposed to obtain

$$\begin{aligned}\mathbf{R} &= E\left\{\mathbf{x}(t)\mathbf{x}^H(t)\right\} \\ &= \mathbf{U}_s\mathbf{\Sigma}_s\mathbf{U}_s^H + \mathbf{U}_n\mathbf{\Sigma}_n\mathbf{U}_n^H\end{aligned} \tag{15}$$

where $\mathbf{\Sigma}_s$ and $\mathbf{\Sigma}_n$ represent the diagonal matrices consisting of K large eigenvalues and 2M + 1 − K small eigenvalues, respectively. $\mathbf{U}_s$ and $\mathbf{U}_n$ denote the signal subspace and noise subspace composed of eigenvectors corresponding to K large eigenvalues and 2M + 1 − K small eigenvalues, respectively.

Considering that the steering vector and noise subspaces are orthogonal, a two-dimensional MUSIC space spectrum about the DOA and range parameters is constructed

$$P(\theta, r) = \left[\mathbf{a}^H(\theta, r)\mathbf{U}_n\mathbf{U}_n^H\mathbf{a}(\theta, r)\right]^{-1} \tag{16}$$

Obviously, when the incident signal is the FFS, range r_k can be considered ∞. At this point, the two-dimensional MUSIC space spectrum can be equated to the one-dimensional MUSIC space spectrum with respect to the DOA parameters under $r_k = \infty$. This means that

$$P(\theta) = \left[\mathbf{a}^H(\theta,\infty)\mathbf{U}_n\mathbf{U}_n^H\mathbf{a}(\theta,\infty)\right]^{-1} \tag{17}$$

The DOA of the K_1 FFSs can be acquired by Equation (17).

3.2. DOA Estimation for NFS

In order to achieve better separation of mixed sources, the oblique projection method is applied to extract the NFS information. Suppose $\mathbf{E}_{\mathbf{A}_F\mathbf{A}_N}$ is an oblique projection operator, whose range space is spanned by $\mathbf{A}_F$ and null space is spanned by $\mathbf{A}_N$ [22]. It possesses the following characteristics [23]:

$$\mathbf{E}_{\mathbf{A}_F\mathbf{A}_N}\mathbf{A}_F = \mathbf{A}_F \tag{18}$$

$$\mathbf{E}_{\mathbf{A}_F\mathbf{A}_N}\mathbf{A}_N = \mathbf{0} \tag{19}$$

Since the DOA of the FFS has been estimated (see Section 3.1), the manifold matrix estimation of the FFS can be gained according to Equations (8) and (13). The oblique projection operator is calculated by [23] as follows:

$$\mathbf{E}_{\mathbf{A}_F\mathbf{A}_N} = \hat{\mathbf{A}}_F\left(\hat{\mathbf{A}}_F^H\mathbf{R}^{\dagger}\hat{\mathbf{A}}_F\right)^{-1}\hat{\mathbf{A}}_F^H\mathbf{R}^{\dagger} \tag{20}$$

We define the pseudo-inverse $\mathbf{R}^{\dagger}$ of covariance matrix $\mathbf{R}$ as:

$$\mathbf{R}^{\dagger} = \sum_{k=1}^{K}\sigma_k^{-1}u_ku_k^H = \mathbf{U}_s\mathbf{\Sigma}_s^{-1}\mathbf{U}_s^H \tag{21}$$

where σ_k indicates the kth large eigenvalue of the covariance matrix $\mathbf{R}$ and u_k represents the eigenvector corresponding to the kth large eigenvalue.

Then, the oblique projection operator $\mathbf{E}_{\mathbf{A}_F\mathbf{A}_N}$ is implemented on the received data, and we have:

$$\begin{aligned}\bar{\mathbf{x}}(t) &= (\mathbf{I}_{2M+1} - \mathbf{E}_{\mathbf{A}_F\mathbf{A}_N})\mathbf{x}(t)\\ &= \mathbf{A}_N\mathbf{s}_N(t) + (\mathbf{I}_{2M+1} - \mathbf{E}_{\mathbf{A}_F\mathbf{A}_N})\mathbf{n}(t)\end{aligned} \tag{22}$$

It can be observed from Equation (22) that the FFS component is suppressed.

Next, a HOC matrix $\mathbf{C}_1$ is constructed from the data with FFS components suppressed. It contains only the NFS DOA information, and its m + M + 1-row n + M + 1-column element is defined as:

$$\begin{aligned}\mathbf{C}_1(m+M+1, n+M+1) &= \mathbf{C}_1'(m,n)\\ &= \mathrm{cum}\{\bar{x}_m(t), \bar{x}_{-m}^*(t), \bar{x}_n^*(t), \bar{x}_{-n}(t)\}\\ &= \sum_{k=1}^{K} c_{4,sk}e^{j(2m-2n)\gamma_k}\end{aligned} \tag{23}$$

where $-M \le m \le M$, $-M \le n \le M$, $c_{4,sk} = \mathrm{cum}\{s_k(t), s_k^*(t), s_k^*(t), s_k(t)\}$ constitute the kurtosis of $s_k(t)$. According to the definition, we can acquire the HOC matrix $\mathbf{C}_1$:

$$\mathbf{C}_1 = \begin{bmatrix}\mathbf{C}_1'(-M,-M) & \mathbf{C}_1'(-M,-M+1) & \cdots & \mathbf{C}_1'(-M,M)\\ \mathbf{C}_1'(-M+1,-M) & \mathbf{C}_1'(-M+1,-M+1) & \cdots & \mathbf{C}_1'(-M+1,M)\\ \vdots & \vdots & \ddots & \vdots\\ \mathbf{C}_1'(M,-M) & \mathbf{C}_1'(M,-M+1) & \cdots & \mathbf{C}_1'(M,M)\end{bmatrix} \tag{24}$$

Equation (24) can be rewritten as

$$\mathbf{C}_1 = \mathbf{B}\mathbf{C}_{4s}\mathbf{B}^H \tag{25}$$

where

$$\mathbf{B} = \left[\mathbf{b}_{K_1+1}, \mathbf{b}_{K_1+2}, \ldots, \mathbf{b}_K\right] \in \mathbb{C}^{(2M+1)\times(K-K_1)} \tag{26}$$

$$\mathbf{b}_k = \left[e^{-j2M\gamma_k}, e^{-j2(M-1)\gamma_k}, \ldots, e^{j2M\gamma_k}\right]^T \in \mathbb{C}^{(2M+1)\times 1} \tag{27}$$

$$\mathbf{C}_{4s} = \mathrm{diag}[c_{4.s_{K_1+1}}, c_{4.s_{K_1+2}}, \ldots, c_{4.s_K}] \in \mathbb{C}^{(K-K_1)\times(K-K_1)} \tag{28}$$

Then we divide $\mathbf{B}$ into two subarrays as shown in the following equation

$$\mathbf{B} = \begin{bmatrix} \mathbf{B}_1 \\ \text{last row} \end{bmatrix} = \begin{bmatrix} \text{first row} \\ \mathbf{B}_2 \end{bmatrix} \tag{29}$$

where

$$\mathbf{B}_1 = [\mathbf{b}_{fr}(\theta_{K_1+1}), \mathbf{b}_{fr}(\theta_{K_1+2}), \ldots, \mathbf{b}_{fr}(\theta_K)] \in \mathbb{C}^{2M\times(K-K_1)} \tag{30}$$

$$\mathbf{B}_2 = [\mathbf{b}_{be}(\theta_{K_1+1}), \mathbf{b}_{be}(\theta_{K_1+2}), \ldots, \mathbf{b}_{be}(\theta_K)] \in \mathbb{C}^{2M\times(K-K_1)} \tag{31}$$

and

$$\mathbf{b}_{fr}(\theta_k) = [e^{-j2M\gamma_k}, \ldots, 1, \ldots, e^{j2(M-1)\gamma_k}]^T \tag{32}$$

$$\mathbf{b}_{be}(\theta_k) = [e^{-j2(M-1)\gamma_k}, \ldots, 1, \ldots, e^{j2M\gamma_k}]^T \tag{33}$$

Clearly, $\mathbf{B}_1$ and $\mathbf{B}_2$ satisfy the following relationship

$$\mathbf{B}_2 = \mathbf{B}_1\mathbf{\Phi} \tag{34}$$

where $\mathbf{\Phi} = \mathrm{diag}\left[\mathrm{e}^{j2\gamma_{K_1+1}}, \ldots, \mathrm{e}^{j2\gamma_K}\right]$.

Performing eigenvalue decomposition for $\mathbf{C}_1$, we have

$$\mathbf{C}_1 = \mathbf{E}_s\mathbf{\Omega}_s\mathbf{E}_s^H + \mathbf{E}_n\mathbf{\Omega}_n\mathbf{E}_n^H \tag{35}$$

where $\mathbf{\Omega}_s$ and $\mathbf{\Omega}_n$ denote the diagonal matrices consisting of $(K-K_1)$ large eigenvalues and $(2M+1-K+K_1)$ small eigenvalues, respectively. $\mathbf{E}_s$ and $\mathbf{E}_n$ represent the signal subspace and noise subspace composed of the eigenvectors corresponding to the $(K-K_1)$ large eigenvalues and $(2M+1-K+K_1)$ small eigenvalues, respectively.

Taking into account that the virtual manifold matrix $\mathbf{B}$ spans the same signal subspace as the eigenvector $\mathbf{E}_s$ corresponding to the large eigenvalues, a non-singular matrix $\mathbf{T}$ exists such that the Equation (36) holds:

$$\mathbf{E}_s = \mathbf{B}\mathbf{T} \tag{36}$$

Similarly, signal subspace $\mathbf{E}_s$ can be divided into two subarrays

$$\mathbf{E}_s = \begin{bmatrix} \mathbf{E}_1 \\ \text{last row} \end{bmatrix} = \begin{bmatrix} \text{first row} \\ \mathbf{E}_2 \end{bmatrix} \tag{37}$$

According to Equations (29), (34), (36) and (37), we have:

$$\mathbf{E}_1 = \mathbf{B}_1\mathbf{T} \tag{38}$$

$$\mathbf{E}_2 = \mathbf{B}_1\mathbf{\Phi}\mathbf{T} \tag{39}$$

Combining Equations (38) and (39), the relationship between $\mathbf{E}_1$ and $\mathbf{E}_2$ can be obtained:

$$\mathbf{E}_2 = \mathbf{E}_1\mathbf{T}^{-1}\mathbf{\Phi}\mathbf{T} = \mathbf{E}_1\mathbf{\Psi} \tag{40}$$

Through Equation (40), we have:

$$\mathbf{\Phi} = \mathbf{T}\mathbf{\Psi}\mathbf{T}^{-1} \tag{41}$$

Observing Equation (41), we can know that $\mathbf{\Phi}$ is equal to the diagonal matrix composed of the eigenvalues of $\mathbf{\Psi}$, and $\mathbf{T}$ is the matrix consisting of the eigenvectors corresponding to the eigenvalues of $\mathbf{\Psi}$. Next, the DOA parameter of NFS can be found by $\mathbf{\Psi}$.

We can solve Equation (41) by using the total least squares method. First, we construct a matrix as follows:

$$\mathbf{E}_{12} = \begin{bmatrix} \mathbf{E}_1 & \mathbf{E}_2 \end{bmatrix} \in \mathbb{C}^{2M \times 2(K-K_1)} \tag{42}$$

Then, we perform singular value decomposition of $\mathbf{E}_{12}$. We define $\mathbf{V} = \mathbf{E}_{12}^H \mathbf{E}_{12}$ as a matrix consisting of right singular vectors, and then divide $\mathbf{V}$ into four $(K-K_1) \times (K-K_1)$-dimensional subarrays as follows:

$$\mathbf{V} = \begin{bmatrix} \mathbf{V}_{11} & \mathbf{V}_{12} \\ \mathbf{V}_{21} & \mathbf{V}_{22} \end{bmatrix} \in \mathbb{C}^{2(K-K_1) \times 2(K-K_1)} \tag{43}$$

Then,

$$\mathbf{\Psi} = -\mathbf{V}_{12}\mathbf{V}_{22}^{-1} \tag{44}$$

After that, we perform eigenvalue decomposition of matrix $\mathbf{\Psi}$ to obtain the $(K-K_1)$ big eigenvalues, and we can acquire the DOA parameter of the $(K-K_1)$ NFSs. The DOA estimation for the kth NFS is expressed as follows:

$$\hat{\theta}_k = \sin^{-1}\left(-\frac{\arg(\psi_k)}{4\pi d/\lambda}\right) \tag{45}$$

where ψ_k denotes the kth large eigenvalue of the rotationally invariant relationship matrix $\mathbf{\Psi}$.

3.3. NFS Range Estimation

Because we acquired the DOA of the NFS (see Section 3.2), the obtained NFS DOA estimation can be substituted into the two-dimensional spatial spectral function (see Section 3.1). The range estimation of NFS can be obtained using just $(K-K_1)$ one-dimensional spectral peak searches. The expression of the kth NFS range parameter estimate is given as follows:

$$\hat{r} = \max_r \left[\mathbf{a}^H(\hat{\theta}_k, r)\mathbf{U}_n\mathbf{U}_n^H\mathbf{a}(\hat{\theta}_k, r)\right]^{-1} \tag{46}$$

Obviously, the DOA and range estimation of NFS have a one-to-one correspondence, and there is no requirement to use an additional parameter matching method.

For clarity, the steps of the proposed algorithm are summarized as follows:

(1) Calculate the covariance matrix of the received data and implement the eigendecomposition on it using Equation (15).
(2) Construct the one-dimensional MUSIC function with Equation (17) for a spectral peak search to obtain an estimation of FFS DOA.
(3) Calculate the oblique projection operator using Equation (20) and apply it to the received data via Equation (22) to obtain the NFS component.
(4) Construct a HOC matrix containing only the NFS DOA information using Equation (23) and implement the eigenvalue decomposition on it with Equation (35) to obtain the signal subspace.
(5) Divide the signal subspace into two overlapping subarrays by Equation (37), and obtain the estimation of NFS DOA using the total least squares method.
(6) Substitute the obtained DOA of NFS into Equation (16) to obtain the MUSIC function about range, and perform several one-dimensional spectral peak searches to obtain the estimation of NFS range.

3.4. Discussion

(1) Maximum number of resolvable mixed sources: From eigenspace theory [5,6], it is well known that the noise and signal subspaces are orthogonal to each other, which is the principle of eigenspace-like algorithms. Therefore, the noise subspace must have at least one eigenvector when eigenvalue decomposition is implemented for the covariance or HOC matrix. Then, the maximum number of estimated signals cannot be more than the minimum value between the number of rows and columns in the constructed matrix [9].

The presented algorithm (as well as TSMUSIC [9], MOS [13], and CMR [14]) builds the $(2M + 1) \times (2M + 1)$-dimensional HOC matrices, and the maximum number of estimated signals is $2M$. In contrast, MBODS [10] uses the spatial smoothing technique for matrix reconstruction in estimating the DOA of NFS, and the maximum number of estimated signals is M. In addition, since both the proposed algorithm and CMR use the ESPRIT-like method, the NFS component matrix is divided into two subarrays of $2M$ rows. If the sources incident to the array are pure NFSs, the maximum number of estimated signals using the presented algorithm, or CMR, is $2M - 1$.

(2) Estimated accuracy: For the DOA estimation of FFS, the presented algorithm (as well as MBODS, MOS, and CMR) uses the one-dimensional MUSIC algorithm directly for covariance data, and the estimation performance is the same. TSMUSIC adopts the high-order MUSIC spectrum search, and the estimation performance is inferior to the other algorithms because the HOC has a larger cumulative error [14]. In addition, if the FFS DOA is estimated using MUSIC theory under the condition of a low signal-to-noise ratio (SNR) or low snapshot number, it is likely that a spurious peak of the NFS will appear. This would undoubtedly affect the estimation performance of the algorithm. For the DOA estimation of NFS, although both the proposed method and the CMR method utilize the ESPRIT-like method, different techniques are used to perform NFS extraction. Both the presented algorithm and the MBODS algorithm use oblique projection, but the former is based on the HOC technique, and the latter utilizes just the inverse diagonal information of the covariance matrix. Therefore, the presented algorithm has superior performance in estimating the DOA of NFS compared to others. For the range estimation of NFS, the presented algorithms, MBODS, MOS, and CMR, all use spectral peak searching. With the higher accuracy of DOA estimation for NFS, the proposed algorithm has superior performance when estimating the range parameter.

(3) Computational complexity: Matrix construction, singular value decomposition, and spectral peak search are the key elements taken into account when assessing algorithm complexity. A $(2M + 1) \times (2M + 1)$-dimensional covariance matrix $\mathbf{R}$ and a $(2M + 1) \times (2M + 1)$-dimensional HOC matrix $\mathbf{C}_1$ are constructed in the proposed algorithm, and eigenvalue decomposition is implemented for these two matrices. Additionally, one angular spectral peak search and $(K - K_1)$ times range spectral peak searches are performed. The complexity of the presented algorithm is $\mathrm{O}(10(2\mathrm{M} + 1)^2\mathrm{N} + 8(2\mathrm{M} + 1)^3/3 + 180\,(2\mathrm{M} + 1)^2/\Delta\theta + (\mathrm{K} - \mathrm{K}_1)\mathrm{F}_\mathrm{r}(2\mathrm{M} + 1)^2)$, where N denotes the snapshot number and $\mathrm{F}_\mathrm{r} = (2\mathrm{D}^2/\lambda - 0.62\,(\mathrm{D}^3/\lambda)^{1/2})/\Delta\mathrm{r}$ is the number of search steps in the Fresnel region. The proposed algorithm has similar computational complexity to the CMR and MBODS algorithms and outperforms the MOS and TSMUSIC algorithms.

4. Numerical Simulations

To evaluate the estimation performance of the presented algorithm, five sets of experiments were performed, which are described in this section. TSMUIC [9], MBODS [10], MOS [13], and CMR [14] were taken as the comparison algorithms. In all five sets of experiments, the number of symmetric uniform array L was fixed at nine, and its array element spacing satisfied $d = \lambda/4$. The incident source was an equal-power statistically independent source $e^{j\delta_t}$, where δ_t is the source phase uniformly distributed between [0, 2π]. The noise is additive zero-mean Gaussian white noise that is statistically independent of the sources. T = 500 independent experiments were performed for each group of experiments. The root mean square error (RMSE) was utilized to assess the estimation performance of each algorithm, and the RMSE of the kth localization parameter is defined as:

$$\mathrm{RMSE}(\alpha_k) = \sqrt{\frac{1}{T}\sum_{j=1}^{T}\left(\alpha_k^j - \alpha_k\right)^2} \tag{47}$$

where α_k^j is the estimated value of the localization parameter for the jth independent experiment and α_k is the true value of the localization parameter.

In the first simulation, the effect of changing the signal-to-noise ratio (SNR) on the estimation performance of each method in the scenario of mixed sources was assessed. Two sources were set up, one each for the FFS and the NFS. The incidence angle of the FFS was 50°. The incidence angle of the NFS was 15°, and the range was 2 λ. The snapshot number N was fixed at 400. The SNR varied from 0 to 30 dB, and 500 independent experiments were conducted at 5 dB intervals. Figures 1 and 2 display the variation of SNR with the RMSE of estimated performance for the mixed source DOA and NFS ranges, respectively. As seen in Figure 1, the estimation capability of the proposed algorithm for the DOA of FFS was equivalent to that of MBODS, CMR, and MOS. The reason is that they all first use a MUSIC search to estimate the FFS DOA. Their precision is significantly greater than that of TSMUSIC. Furthermore, the RMSE of the NFS DOA estimation with the presented algorithm is smaller than other compared algorithms. Although the proposed algorithm and the CMR method both use the ESPRIT-like algorithm to estimate the DOA of NFS, they adopt different methods to separate NFS and FFS. According to the experiments, the proposed algorithm uses oblique projection, which is more effective than the matrix difference technique in the CMR method. As seen in Figure 2, the presented method also outperformed the other algorithms in estimating the range of NFS. Although MBODS, MOS, and CMR all obtain range estimation by spectral peak search, the performance of the presented method in estimating the DOA of NFS is superior, so the method is more advantageous for subsequent range estimation.

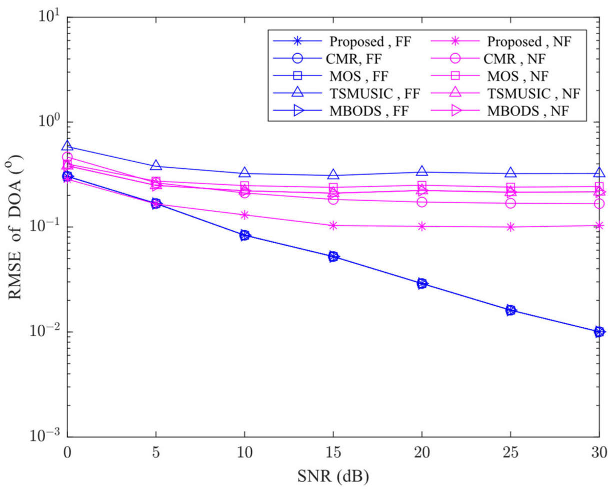

Figure 1. Comparison of estimation for DOA with varying SNR in first experiment (N = 400, (50°, ∞), (15°, 2 λ)).

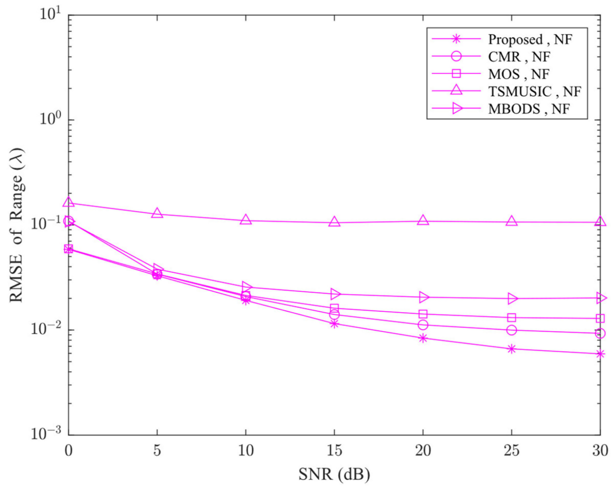

Figure 2. Comparison of estimation for range with varying SNR in first experiment (N = 400, (50°, ∞), (15°, 2 λ)).

In the second simulation, we assessed the effect of the varying snapshot number on the estimation performance of each method considering the mixed source scenario. The source configuration was identical to that of the previous experiment. The SNR was fixed at 15 dB. The snapshot number varied from 200 to 2000, and 500 Monte Carlo simulations were carried out at intervals of 200 snapshots. Figures 3 and 4 show the variation of RMSE with snapshot number for the estimation performance of mixed sources in the DOA and NFS ranges, respectively. As can be seen in Figure 3, the presented algorithm obviously surpasses the other algorithms in estimating the DOA of NFS. As shown in Figure 4, the proposed algorithm and MOS have better performance in estimating the NFS range at low snapshot numbers. With the increasing number of snapshots, the proposed algorithm outperforms the others and has comparable performance to the CMR algorithm. There is an order in the RMSE of CMR at 200 to 400 snapshots, which may be due to the small data sample and a large bias in the estimated performance.

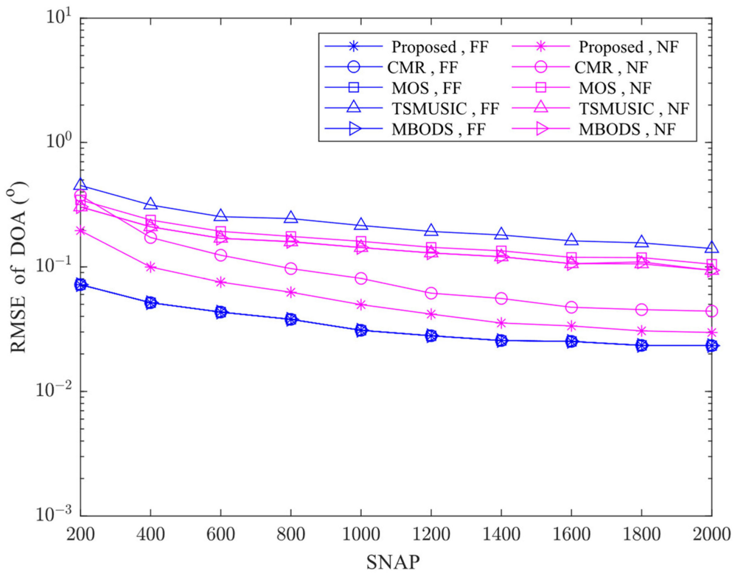

Figure 3. Comparison of estimation for DOA with varying snapshots in second experiment (SNR = 15, (50°, ∞), (15°, 2 λ)).

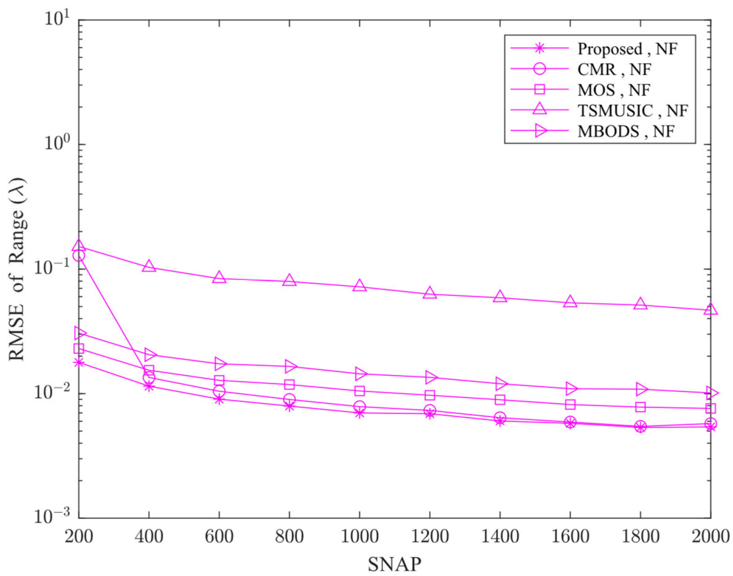

Figure 4. Comparison of estimation for range with varying snapshots in second experiment (SNR = 15, (50°, ∞), and (15°, 2 λ)).

In the third experiment, we analyzed the effect of varying SNR on estimating localization parameters with each algorithm in the pure NFS scenario. Two NFSs were assumed to be incidental to the array. The angle of the first NFS was 10°, and its range was 2λ. The angle of the second NFS was 45°, and its range was 3.5 λ. The snapshot number N was fixed at 400. The SNR was changed from 0 to 30 dB, and 500 independent simulations were conducted at 5 dB intervals. Figures 5 and 6 show the RMSE of estimation performance with varying SNR for the DOA and the range of pure NFSs, respectively. As shown in Figure 5, the performance variation curves of the presented algorithm and the CMR algorithm are equivalent. Because both algorithms use the ESPRIT-like algorithm for NFS DOA estimation and the received array sources are pure NFSs, the previous steps of the algorithm process are invalid. In addition, the variation curves of MOS and MBODS overlap because both use the high-order MUSIC method. From Figure 6, we can see that both the proposed algorithm and CMR are more advantageous at a high SNR and estimate the range parameter of the NFS more accurately.

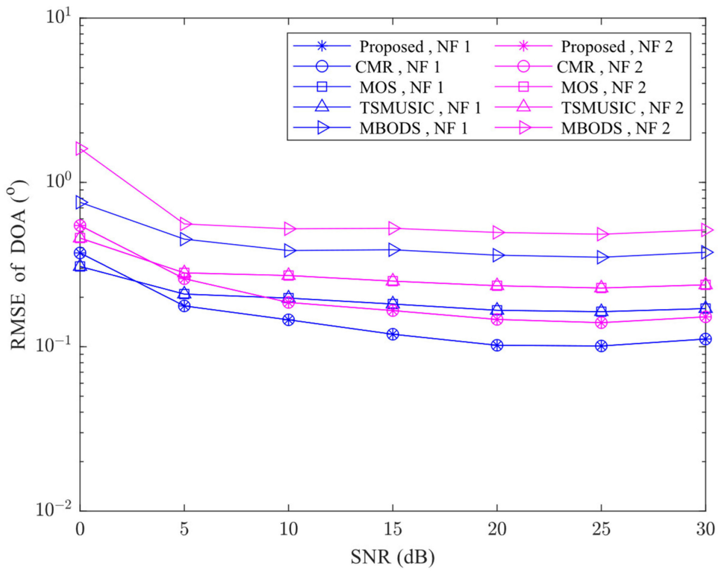

Figure 5. Comparison of estimation for DOA with varying SNR in third experiment (N = 400, (10°, 2 λ), (45°, 3.5 λ)).

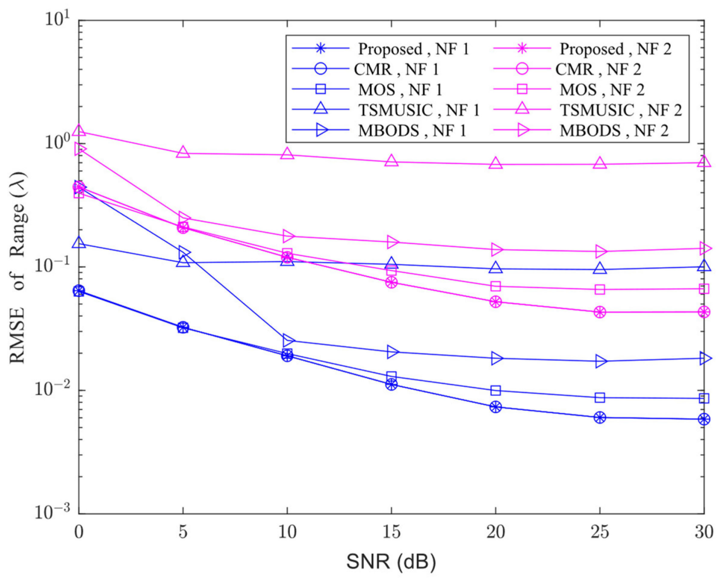

Figure 6. Comparison of estimation for range with varying SNR in third experiment (N = 400, (10°, 2 λ), (45°, 3.5 λ)).

In the fourth experiment, we assessed the effect of changing the snapshot number on the estimation performance of each method in the pure NFS scenario. The source setting was identical to that of the third simulation. The SNR was fixed at 15 dB. The snapshot number was changed from 200 to 2000, and 500 independent experiments were conducted at intervals of 200 snapshots. Figures 7 and 8 show the estimated performance of the RMSE with the varying snapshot numbers for the DOA and the range of pure NFSs, respectively. Figure 7 shows that the presented algorithm and CMR had better performance in NFS DOA estimation with the 2000 snapshot. According to Figure 8, the proposed algorithm and CMR have similar performance to MOS and outperform the other algorithms.

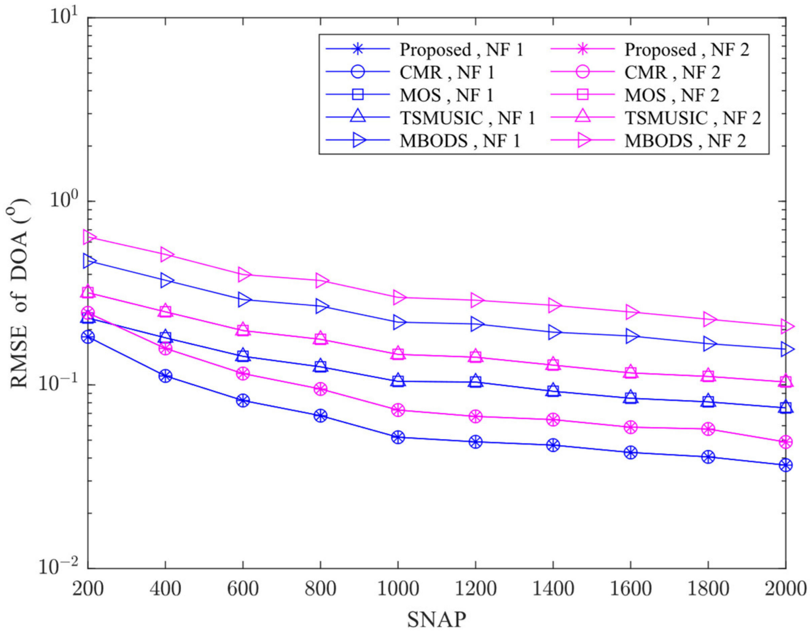

Figure 7. Comparison of estimation for DOA with varying snapshots in fourth experiment (SNR = 15, (10°, 2 λ), (45°, 3.5 λ)).

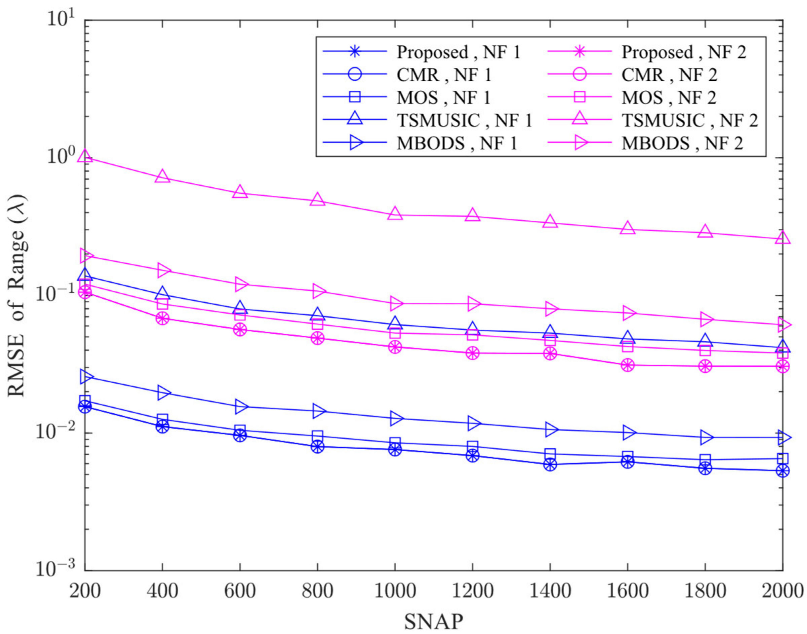

Figure 8. Comparison of estimation for range with varying snapshots in fourth experiment (SNR = 15, (10°, 2 λ), (45°, 3.5 λ)).

In the fifth simulation, the computational complexity of each method for different numbers of snapshots was verified. The experimental configuration was the same as in the second simulation. The angle search interval was 0.01°, and the range search interval was 0.01 λ. Figure 9 illustrates the variation in computational complexity of each algorithm with snapshot numbers. As shown in Figure 9, the presented algorithm and CMR have comparable computational complexity, which is similar to the MBODS algorithm, and they outperform MOS and TSMUSIC. The computational complexity of TSMUIC is too high with a high snapshot number.

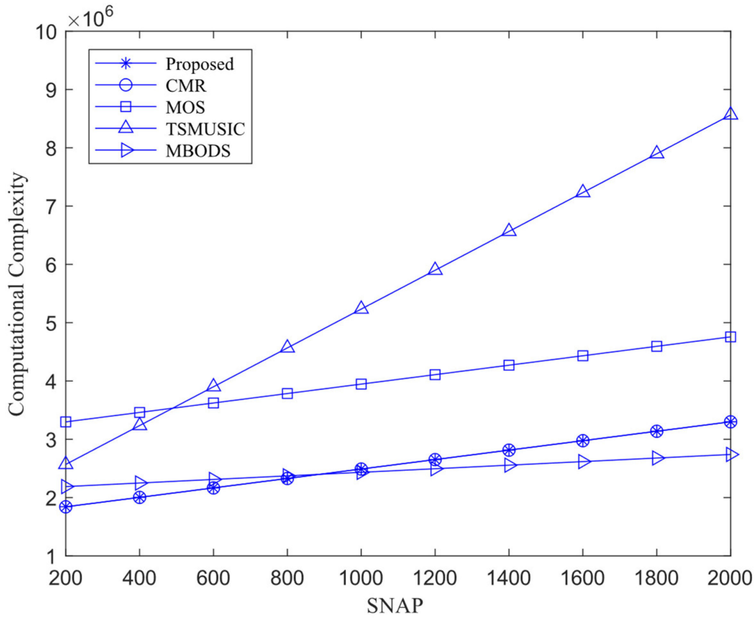

Figure 9. Comparison of computational complexity with varying snapshots in the fifth experiment.

5. Conclusions

In this paper, a mixed source localization algorithm based on oblique projection and HOC techniques is presented. The DOA of FFS is first acquired by the MUSIC method. The FFS component is suppressed by oblique projection, and the NFS component is extracted from the received array data. The separation effect is better than that of the CMR algorithm. The array elements of a particular sequence are chosen to build a HOC matrix without a range factor, and the DOA of NFS is calculated using the ESPRIT-like method. Finally, the NFS range is ascertained through a MUSIC search. The proposed algorithm effectively improves the estimation of NFS parameters with the same performance as the high-precision estimation for the FFS DOA. Experiments were conducted to illustrate the superiority of the presented algorithm in both pure NFS and mixed source scenarios.

Author Contributions: Conceptualization, H.S. and Y.Y.; methodology, H.S. and Y.Y.; software, Y.Y. and G.Y.; validation, H.S., Y.Y. and G.Y.; formal analysis, S.W.; writing—review and editing, H.S., Y.Y. and S.W.; supervision, H.S. All authors have read and agreed to the published version of the manuscript.

Funding: This research was funded by the Scientific Research Project of the Tianjin Municipal Education Commission, grant number 2021KJ016.

Data Availability Statement: Not applicable.

Conflicts of Interest: The authors declare no conflict of interest. The funders had no role in the design of the study; in the collection, analyses, or interpretation of data; in the writing of the manuscript; or in the decision to publish the results.

References

1. Krim, H.; Viberg, M. Two decades of array signal processing research: The parametric approach. *IEEE Signal Process. Mag.* **1996**, *13*, 67–94. [CrossRef]
2. Chen, H.; Jiang, Z.; Liu, W.; Tian, Y.; Wang, G. Conjugate augmented decoupled 3-D parameters estimation method for near-field sources. *IEEE Trans. Aerosp. Electron. Syst.* **2022**, *58*, 4681–4689. [CrossRef]
3. Van Trees, H.L. *Optimum Array Processing: Part IV of Detection, Estimation, and Modulation Theory*; John Wiley & Sons: Hoboken, NJ, USA, 2002.
4. Schmidt, R. Multiple emitter location and signal parameter estimation. *IEEE Trans. Antennas Propag.* **1986**, *34*, 276–280. [CrossRef]
5. Roy, R.; Kailath, T. ESPRIT-estimation of signal parameters via rotational invariance techniques. *IEEE Trans. Acoust. Speech Signal Process.* **1989**, *37*, 984–995. [CrossRef]
6. Chen, H.; Wang, W.; Liu, W. Joint DOA, range, and polarization estimation for rectilinear sources with a cold array. *IEEE Wirel. Commun. Lett.* **2019**, *8*, 1398–1401. [CrossRef]
7. Huang, Y.D.; Barkat, M. Near-field multiple source localization by passive sensor array. *IEEE Trans. Antennas Propag.* **1991**, *39*, 968–975. [CrossRef]
8. Jiang, Z.; Chen, H.; Liu, W.; Wang, G. 3D temporal-spatial-based near-field source localization considering amplitude attenuation. *Signal Process.* **2022**, *201*, 108735. [CrossRef]
9. Liang, J.; Liu, D. Passive localization of mixed near-field and far-field sources using two-stage MUSIC algorithm. *IEEE Trans. Signal Process.* **2009**, *58*, 108–120. [CrossRef]
10. He, J.; Swamy, M.N.S.; Ahmad, M.O. Efficient application of MUSIC algorithm under the coexistence of far-field and near-field sources. *IEEE Trans. Signal Process.* **2011**, *60*, 2066–2070. [CrossRef]
11. Liu, G.; Sun, X. Efficient method of passive localization for mixed far-field and near-field sources. *IEEE Antennas Wirel. Propag. Lett.* **2013**, *12*, 902–905. [CrossRef]
12. Wang, K.; Wang, L.; Shang, J.R.; Qu, X.X. Mixed near-field and far-field source localization based on uniform linear array partition. *IEEE Sens. J.* **2016**, *16*, 8083–8090. [CrossRef]
13. Zheng, Z.; Sun, J.; Wang, W.Q.; Yang, H. Classification and localization of mixed near-field and far-field sources using mixed-order statistics. *Signal Process.* **2018**, *143*, 134–139. [CrossRef]
14. Zheng, Z.; Fu, M.; Jiang, D.; Wang, W.Q.; Zhang, S. Localization of mixed far-field and near-field sources via cumulant matrix reconstruction. *IEEE Sens. J.* **2018**, *18*, 7671–7680. [CrossRef]
15. Yuen, N.; Friedlander, B. Performance analysis of higher order ESPRIT for localization of near-field sources. *IEEE Trans. Signal Process.* **1998**, *46*, 709–719. [CrossRef]
16. Molaei, A.M.; Zakeri, B.; Andargoli, S.M.H. Passive localization and classification of mixed near-field and far-field sources based on high-order differencing algorithm. *Signal Process.* **2019**, *157*, 119–130. [CrossRef]
17. Wu, X.; Yan, J. 3-D mixed far-field and near-field sources localization with cross array. *IEEE Trans. Veh. Technol.* **2020**, *69*, 6833–6837. [CrossRef]
18. Yin, K.; Dai, Y.; Gao, C. Mixed near-field and far-field source localization using COLD arrays. *Circuits Syst. Signal Process.* **2022**, *41*, 3642–3655. [CrossRef]
19. Wang, B.; Liu, J.; Sun, X. Mixed sources localization based on sparse signal reconstruction. *IEEE Signal Process. Lett.* **2012**, *19*, 487–490. [CrossRef]
20. Tian, Y.; Lian, Q.; Xu, H. Mixed near-field and far-field source localization utilizing symmetric nested array. *Digit. Signal Process.* **2018**, *73*, 16–23. [CrossRef]
21. Zheng, Z.; Fu, M.; Wang, W.Q.; Zhang, S.; Liao, Y. Localization of mixed near-field and far-field sources using symmetric double-nested arrays. *IEEE Trans. Antennas Propag.* **2019**, *67*, 7059–7070. [CrossRef]
22. McCloud, M.L.; Scharf, L.L. A new subspace identification algorithm for high-resolution DOA estimation. *IEEE Trans. Antennas Propag.* **2002**, *50*, 1382–1390. [CrossRef]
23. Behrens, R.T.; Scharf, L.L. Signal processing applications of oblique projection operators. *IEEE Trans. Signal Process.* **1994**, *42*, 1413–1424. [CrossRef]